Inelastic processes in calcium-hydrogen ionic collisions with account for fine structure

A. K. Belyaev,* Ya. V. Voronov, and S. A. Yakovleva
Department of Theoretical Physics and Astronomy, Herzen University, St. Petersburg 191186, Russia

(Received 28 October 2019; published 20 December 2019)

Inelastic processes in low-energy $Ca^+ + H$ and $Ca^{2+} + H^-$ collisions accounting for the fine structure of calcium ions are investigated. The present study is based on *ab initio* nonrelativistic potentials and on modification of the potentials by switching the representation from the *LS* to the *JJ* coupling scheme. The nuclear dynamical study is performed by the multichannel Landau-Zener approach for the collisional energy range 10^{-4} to 100 eV. The rate coefficients are calculated for the temperature range 1000 to 10 000 K. It is found that the largest rate coefficients correspond to the neutralization processes into the final channels $Ca^+(4f\,^2F^\circ_{7/2})$, $Ca^+(6s\,^2S_{1/2})$, $Ca^+(5d\,^2D_{3/2,5/2})$, $Ca^+(6p\,^2P^\circ_{1/2,3/2})$, and $Ca^+(7s\,^2S_{1/2}) + H(1s\,^2S_{1/2})$, at a temperature of 6000 K they have values exceeding 10^{-8} cm^3 s^{-1}, and the reaction mechanism for these processes corresponds to the long-range ionic-covalent interaction. The rate coefficients for the Ca II infrared triplet 849.8/854.2/866.2-nm transitions in collisions with H are found to be small. It is shown that accounting for the fine structure does not lead to a simple redistribution of rate coefficients obtained within the *LS* coupling scheme between the fine-structure levels.

DOI: 10.1103/PhysRevA.100.062710

I. INTRODUCTION

Determination of reaction mechanisms and calculations of cross sections and rate coefficients of inelastic processes in atomic collisions are of fundamental importance in modern atomic and molecular physics since inelastic collision processes govern properties of gas and plasma medium. In particular, this detailed and complete information is required for non–local thermodynamic equilibrium (non-LTE) modelings of stellar spectra, which are in turn used for one of the fundamental problems in modern astrophysics, determination of stellar absolute and relative chemical abundances (see, e.g., reviews [1–4]). It is known that the important processes for these purposes are those that take place in collisions of heavy particles with hydrogen atoms and anions due to the highest abundance of hydrogen in the Universe. The lack of reliable information on inelastic processes in collisions of atoms and positive ions of a treated chemical element with hydrogen atoms and negative ions, causes the main uncertainty in non-LTE modelings. For a long while, in the absence of quantum calculations, cross sections and rate coefficients for inelastic processes in collisions with hydrogen were estimated by the classical so-called Drawin formula [5–7], until it was recognized that this formula is not reliable [8]: For optically allowed transitions the formula overestimates cross sections by up to several orders of magnitude, and for optically forbidden transitions it underestimates cross sections by up to several orders of magnitude, compared with full quantum data. Therefore, it has been commonly realized that H-collision cross sections obtained by full quantum or model quantum calculations are needed.

Significant progress has been achieved during the last two decades through detailed full-quantum H-scattering calculations, based on accurate quantum chemical data, for the cases of Na, Li, H, Mg, He, and Ca [9–21]. These calculations have demonstrated the importance of the ionic-covalent avoided crossing mechanism, although other reaction mechanisms have been tested as well. The long-range ionic-covalent mechanism determines inelastic H-collision rate coefficients with large and moderate values, that is, for the processes of importance for non-LTE modelings. Nevertheless, full-quantum calculations are still rather rare and time-consuming, and hence, model quantum approaches for treating both electronic structures and nonadiabatic nuclear dynamics are highly desired. As a result, several quantum approaches have been developed, in particular, based on long-range ionic-covalent interactions: the asymptotic semiempirical approach [22], the asymptotic linear combination of atomic orbitals [23],[1] the simplified method [25,26], the multichannel Landau-Zener approach [27–29], and the hopping probability current method [22]. These model approaches have been successfully applied to a number of inelastic processes in collisions of different chemical elements with hydrogen: Al, Si, Be, Mn, K, Rb, Ca, Ca^+, Ba, Ba^+, Fe, Fe^+, Li, O, C, and N (see, e.g., [21], [23], and [30–36], and references therein).

Within these approaches both electronic structures and nonadiabatic nuclear dynamics are treated in the *LS*-coupling scheme, that is, without accounting for the fine structure, although transitions between fine-structure levels are also of astrophysical interest. For example, the Ca II infrared triplet (849.8, 854.2 and 866.2 nm) is of particular interest for studying radial velocities and metallicities of distant stars and stellar systems [37–41]. This triplet

*andrey.k.belyaev@gmail.com

[1]See [24] for Erratum.

corresponds to transitions between the following fine-structure states: $Ca^+(4p,\ ^2P^\circ_{3/2}) \rightarrow Ca^+(3d\,^2D_{3/2})$, $Ca^+(4p\,^2P^\circ_{3/2}) \rightarrow Ca^+(3d\,^2D_{5/2})$, and $Ca^+(4p\,^2P^\circ_{1/2}) \rightarrow Ca^+(3d\,^2D_{3/2})$. For this reason, special attention is given in the present work to the inelastic processes in collisions of calcium ions with hydrogen atoms and anions involving these fine-structure states of Ca II.

In general, calcium is an important element for astrophysical observations [1,4]. It is one of the best observable chemical elements in late-type stars [42–44]. In the case of extremely metal-poor stars, Ca is the only chemical element that is visible in the two ionization stages [42]. Calcium is also important for astrophysical observations because it belongs to the α-element group and can help us to distinguish stellar populations in the Galactic disk and halo and to understand the link to dwarf spheroidal galaxies (see [43], [45], and [46], and references therein).

Several non-LTE modelings of stellar spectra have been performed for both the calcium atom [37,42–44,47–56] and the calcium ion [37,42–44,56–61] (see also references therein). Inelastic processes in collisions of hydrogen with neutral calcium have been studied in several papers [16,21,23,24,30,62], while collisions of hydrogen with single-ionized Ca^+ have been treated in only one paper [31]. The results of these studies have been applied to non-LTE modeling of the Ca I spectrum [37,43,44].[2]

Although inelastic processes in $Ca + H$, $Ca^+ + H^-$, $Ca^+ + H$, and $Ca^{2+} + H^-$ collisions were studied in detail, the aforementioned studies did not consider fine-structure levels.

It is useful to point out that in the absence of more accurate estimates, the common way to take into account the fine structure in H collisions consists in redistributing the collisional rate coefficient between fine-structure levels [63]. Another approach to account for the fine structure is developed in the present paper. The approach is based on a transformation of adiabatic molecular potentials upon changing the representation from the *LS* coupling scheme to the *JJ* one. In the present paper, this approach is applied to accounting for fine-structure levels in $Ca^+ + H$ and $Ca^{2+} + H^-$ collisions.

II. BRIEF THEORY

The present treatment is performed in the framework of the Born-Oppenheimer approach, which considers a scattering problem in two steps: (i) the electronic structure of a corresponding molecule at fixed nuclei and (ii) nonadiabatic nuclear dynamics. The fixed-nuclei electronic structure can be determined if diabatic (diagonal) potentials and diabatic off-diagonal matrix elements of an electronic Hamiltonian are known. The diabatic representation allows one to determine the Landau-Zener parameters for avoided-crossing regions or adiabatic potentials, which also lead to the determination of Landau-Zener parameters. In the present case, the most important is determination of long-range off-diagonal ionic-covalent matrix elements. Accounting for the fine structure is currently proposed by switching from the *LS* coupling scheme to the *JJ* one. This finally leads to determination of the inelastic transition probabilities, inelastic cross sections, and rate coefficients accounting for the fine structure. They are computed as follows.

The present study is based on the *ab initio* potential energies of the CaH^+ molecular ion computed by Habli *et al.* [65,66] in the *LS* representation. The *LS* representation deals with the nonrelativistic electronic Hamiltonian $H_e^{\rm nr}$ and nonrelativistic electronic wave functions $|L\tilde{\Lambda}Sm_S\rangle_{LS}$ (see, e.g., [67]). In the cases of alkali atoms and alkali-earth ions A^+ interacting with H, we are interested in ionic $A^{2+}(^1S) + H^-(^1S)$ and covalent $A^+(nl\ ^2L) + H(^2S)$ configurations of the same molecular symmetry with the corresponding molecular wave functions $|0000\rangle_{LS}$ and $|L000\rangle_{LS}$, respectively. In the *LS* representation, the ionic molecular state has $^1\Sigma^+$ symmetry, so only covalent states with the same molecular symmetry are currently treated. Taking proper nonrelativistic wave functions for a diabatic representation, one can construct diagonal and off-diagonal Hamiltonian matrix elements in the form of diagonal ionic and covalent potentials and off-diagonal ionic-covalent couplings. Such a representation expresses the long-range ionic-covalent interaction mechanism. In this approach, the key point is determination of the off-diagonal coupling matrix elements $\langle 0000|H_e^{\rm nr}|L000\rangle_{LS}$. Within the semiempirical asymptotic approach [22], these matrix elements can be determined by the couplings $H_{LS}^{\rm Olson}$ computed by means of the semiempirical Olson-Smith-Bauer formula [68]

$$\langle 0000|H_e^{\rm nr}|L000\rangle_{LS} = H_{LS}^{\rm Olson}\,. \tag{1}$$

Knowing the Hamiltonian matrix in the *LS* representation, that is, the diagonal and off-diagonal matrix elements, one can calculate the nonrelativistic adiabatic potentials, as well as the nonadiabatic couplings, and this allows one to perform complete quantum or model quantum treatments of nonadiabatic nuclear dynamics and, finally, to calculate the inelastic transition probabilities, cross sections, and rate coefficients.

In order to take into account fine-structure states for the ionic-covalent interaction, one needs to treat a (quasi-) relativistic Hamiltonian $H_e^{\rm rel}$ and to use molecular wave functions in the *JJ* representation, $|J_1, J_2; J\Omega\rangle_{JJ}$. A (quasi-) relativistic Hamiltonian deviates from a nonrelativistic one by relativistic operators $V^{\rm rel}$, first, the spin-orbit operators $V^{\rm so}$,

$$H_e^{\rm rel} = H_e^{\rm nr} + V^{\rm rel}\,. \tag{2}$$

Diagonal matrix elements of the relativistic operators $V^{\rm rel}$, Eq. (2), calculated on diabatic molecular wave functions in the *JJ* representation, provide fine-structure level shifts in a diabatic representation. These shifts can be taken from experimental data, e.g., from NIST [64], and this allows one to determine diabatic potentials with proper fine-structure asymptotes. Off-diagonal matrix elements of the (quasi-)relativistic Hamiltonian calculated on the same molecular wave functions yield ionic-covalent couplings and have the form of the sum of two terms: matrix elements of a nonrelativistic Hamiltonian and matrix elements of the relativistic operators. Typically, the latter are much smaller than the former, and hence, we assume that the off-diagonal matrix elements of the relativistic operators can be omitted. Therefore, the off-diagonal matrix elements of the (quasi-)relativistic Hamiltonian are

[2]In these non-LTE modelings, the rates for H + Ca II collisional processes were determined by the classical Drawin formula or neglected completely.

TABLE I. $CaH^+(k\ 0^+)$ molecular states (in the JJ representation), the corresponding scattering channels, their asymptotic energies with respect to the ground-state level (taken from NIST [64]), and the statistical probabilities $p_k^{\rm stat}$ for populations of the molecular states 0^+.

k	Scattering channels	Asymptotic energy (eV)	$p_k^{\rm stat}$
1	$Ca^+(4s\,^2S_{1/2}) + H(1s\,^2S_{1/2})$	0.0	0.25
2	$Ca^+(3d\,^2D_{3/2}) + H(1s\,^2S_{1/2})$	1.692408	0.125
3	$Ca^+(3d\,^2D_{5/2}) + H(1s\,^2S_{1/2})$	1.699932	0.0833
4	$Ca^+(4p\,^2P^\circ_{1/2}) + H(1s\,^2S_{1/2})$	3.123349	0.25
5	$Ca^+(4p\,^2P^\circ_{3/2}) + H(1s\,^2S_{1/2})$	3.150984	0.125
6	$Ca^+(5s\,^2S_{1/2}) + H(1s\,^2S_{1/2})$	6.467875	0.25
7	$Ca^+(4d\,^2D_{3/2}) + H(1s\,^2S_{1/2})$	7.047169	0.125
8	$Ca^+(4d\,^2D_{5/2}) + H(1s\,^2S_{1/2})$	7.049551	0.0833
9	$Ca^+(5p\,^2P^\circ_{1/2}) + H(1s\,^2S_{1/2})$	7.505138	0.25
10	$Ca^+(5p\,^2P^\circ_{3/2}) + H(1s\,^2S_{1/2})$	7.514841	0.125
11	$Ca^+(4f\,^2F^\circ_{5/2}) + H(1s\,^2S_{1/2})$	8.437981	0.0833
12	$Ca^+(4f\,^2F^\circ_{7/2}) + H(1s\,^2S_{1/2})$	8.437981	0.0625
13	$Ca^+(6s\,^2S_{1/2}) + H(1s\,^2S_{1/2})$	8.762908	0.25
14	$Ca^+(5d\,^2D_{3/2}) + H(1s\,^2S_{1/2})$	9.016407	0.125
15	$Ca^+(5d\,^2D_{5/2}) + H(1s\,^2S_{1/2})$	9.017486	0.0833
16	$Ca^+(6p\,^2P^\circ_{1/2}) + H(1s\,^2S_{1/2})$	9.234953	0.25
17	$Ca^+(6p\,^2P^\circ_{3/2}) + H(1s\,^2S_{1/2})$	9.239519	0.125
18	$Ca^+(7s\,^2S_{1/2}) + H(1s\,^2S_{1/2})$	9.850331	0.25
19	$Ca^+(4s\,^2S_{1/2}) + H(2s\,^2S_{1/2})$	10.20165	0.25
20	$Ca^+(4s\,^2S_{1/2}) + H(2p\,^2P_{1/2})$	10.20505	0.25
21	$Ca^+(4s\,^2S_{1/2}) + H(2p\,^2P_{3/2})$	10.20505	0.125
22	$Ca^{2+}(3p^6\,^1S_0) + H^-(1s^2\,^1S_0)$	11.11772	1.0

mainly determined by the off-diagonal matrix elements of the nonrelativistic Hamiltonian calculated on the molecular wave functions in the JJ representation. In this representation, the ionic configuration $A^{2+}(^1S_0) + H^-(^1S_0)$ has 0^+ symmetry, so the covalent molecular states $A^+(nl\ ^2L_j) + H(^2S_{1/2})$ included in consideration should have the same symmetry. Table I lists the molecular states with this symmetry and treated in the present work. Both ionic and covalent molecular wave functions can be expressed via the single-electronic wave functions. It turns out that the off-diagonal matrix elements calculated on the molecular wave functions in the LS and in the JJ representations are proportional to each other [69],

$$\langle 0,\ 0;\ 0\,0\,|\,H_e^{\rm rel}\,|\,j,\ {}^1/_2;\ J\,0\rangle_{JJ} = C\,\langle 0000|H_e^{\rm nr}|L000\rangle_{LS}\,, \tag{3}$$

where the proportionality factors C are equal to

$$C = \frac{1}{\sqrt{2}}\left(\begin{bmatrix} j & {}^1/_2 & J \\ {}^1/_2 & {}^{-1}/_2 & 0 \end{bmatrix}\begin{bmatrix} l & {}^1/_2 & j \\ 0 & {}^1/_2 & {}^1/_2 \end{bmatrix} - \begin{bmatrix} j & {}^1/_2 & J \\ {}^{-1}/_2 & {}^1/_2 & 0 \end{bmatrix}\begin{bmatrix} l & {}^1/_2 & j \\ 0 & {}^{-1}/_2 & {}^{-1}/_2 \end{bmatrix}\right), \tag{4}$$

where the brackets denote the Clebsch-Gordan coefficients. The proportionality factors for several fine-structure states are listed in Table II. Note that J is the total electronic angular momentum quantum number for a covalent configuration, $A^+(nl\ ^2L_j) + H(^2S_{1/2})$, of a (quasi-)molecule AH^+ at present and is obtained as the sum of two atomic total angular momenta with the quantum numbers j and $1/2$.

TABLE II. Proportionality factors C between off-diagonal matrix elements in the JJ and in the LS representations for several fine-structure levels.

L	j	J	C	L	j	J	C
S	${}^1/_2$	0	1	P	${}^1/_2$	0	0
	${}^1/_2$	1	0		${}^1/_2$	1	$-\sqrt{{}^1/_3}$
					${}^3/_2$	1	$\sqrt{{}^2/_3}$
					${}^3/_2$	2	0
D	${}^3/_2$	1	0	F	${}^5/_2$	2	0
	${}^3/_2$	2	$-\sqrt{{}^2/_5}$		${}^5/_2$	3	$-\sqrt{{}^3/_7}$
	${}^5/_2$	2	$\sqrt{{}^3/_5}$		${}^7/_2$	3	$\sqrt{{}^4/_7}$
	${}^5/_2$	3	0		${}^7/_2$	4	0

The diabatic potentials in the JJ representation can be taken in the same way as those in the LS representation, but the asymptotes of the covalent potentials coincide with the corresponding fine-structure levels. Thus, knowing the diabatic diagonal and off-diagonal matrix elements of the electronic Hamiltonian allows one to calculate the adiabatic (quasi-)relativistic potentials based on the long-range ionic-covalent interaction and, therefore, to compute the inelastic state-to-state probabilities, cross sections, and rate coefficients, e.g., by the asymptotic multichannel approach. It is noteworthy that the number of molecular states in the JJ representation is greater than the number of states in the LS representation due to splitting of nonrelativistic levels into fine-structure levels. An important feature is that both the off-diagonal ionic-covalent matrix elements $\langle 0,\ 0;\ 0\,0\,|\,H_e^{\rm rel}\,|\,j,\ {}^1/_2;\ J\,0\rangle_{JJ}$ (which determine the Landau-Zener parameters) and the energy splittings in the avoided-crossing regions are smaller in the JJ representation than in the LS one [see Eqs. (3) and (4) and Table II]. One can see another feature: due to the properties of the Clebsch-Gordan coefficients, for (nearly) degenerate covalent 0^+ states the following relation is fulfilled at a fixed L:

$$\sum_j \langle 0,\ 0;\ 0\,0\,|\,H_e^{\rm rel}\,|\,j,\ {}^1/_2;\ J\,0\rangle_{JJ}^2 = \langle 0000|H_e^{\rm nr}|L000\rangle_{LS}^2\,. \tag{5}$$

Note that $C = 0$ for the 0^- symmetry. Due to Eq. (5), the outermost adiabatic potentials in a nonadiabatic region created by an ionic state and two fine-structure covalent states in the JJ representation coincide with the similar adiabatic potentials in the LS representation, but in the JJ representation there is an additional potential in between (see the example shown in Fig. 1).

In the present case, the adiabatic *ab initio* CaH^+ potentials have been calculated in the LS representation of Habli *et al.* [65,66]. Using their potentials, the inelastic processes in low-energy $Ca^+ + H$ and $Ca^{2+} + H^-$ collisions have been studied in a recent paper [31] without accounting for fine-structure

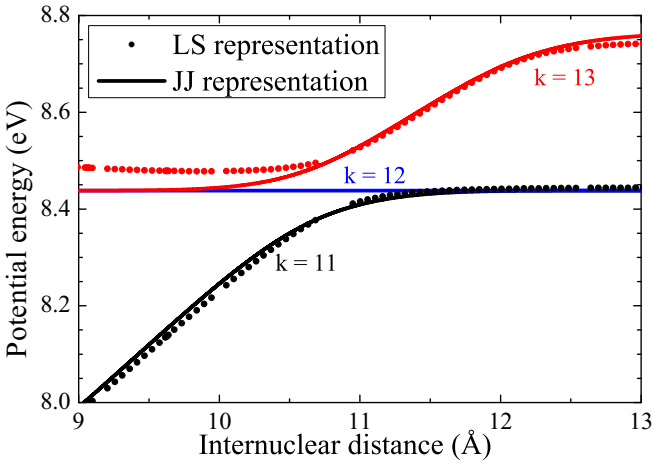

FIG. 1. Adiabatic potentials for the molecular states $k = 11$, 12, and 13 (see Table I) in the JJ representation (solid lines, with account for the fine structure), as well as in the LS representation (dotted lines, without the fine structure).

states. It was shown in that paper that large-valued rate coefficients correspond to processes based on the long-range ionic-covalent interaction. Thus, in order to take the fine structure into account for the most important processes (with large rate coefficients) one can use the approach described above and apply it to the long-range nonadiabatic regions.

In order to account for the fine structure, the *ab initio* $CaH^+(^1\Sigma^+)$ potentials in the LS representation are used to determine the diabatic diagonal and the off-diagonal $\langle 0000|H_e^{\rm nr}|L000\rangle_{LS}$ matrix elements of the electronic Hamiltonian in each long-range avoided-crossing region. In the JJ representation, the long-range electronic Hamiltonian matrix is constructed in the following way: (i) the diabatic diagonal elements are taken in the same way as the corresponding diabatic potentials in the LS representation, but split and shifted to the proper fine-structure level asymptotes; and (ii) the diabatic off-diagonal elements $\langle 0,\ 0;\ 0\,0\,|\,H_e^{\rm rel}\,|\,j,\ {}^1/_2;\ J\,0\rangle_{JJ}$ are calculated by means of Eq. (3) via the factors C in Eq. (4) (see Table II) and the nonrelativistic matrix elements $\langle 0000|H_e^{\rm nr}|L000\rangle_{LS}$. The latter can be either determined by the adiabatic potential splittings in the LS representation or calculated directly, e.g., by Eq. (1). Note that the number of fine-structure scattering channels is greater than the number of LS channels due to the splittings of the LS levels. In the present work, we take into account 22 fine-structure scattering channels producing the molecular states of 0^+ symmetry, 21 covalent, $Ca^+(nl\,^2L_j) + H(^2S_{1/2})$, and one ionic, $Ca^{2+}(^1S_0) + H^-(^1S_0)$ (see Table I), which are based on the 14 scattering channels in the LS representation, 13 covalent and one ionic.

It is noteworthy that the present consideration does not include states corresponding to $Ca + H^+$ channels. First, inelastic processes involving these states correspond to two-electron transitions with cross sections and rate coefficients typically being low if other reaction mechanisms are not involved. Second, these states do not correspond to alkaline-like–neutral-hydrogen interactions, so the wave function transformation [69] is not directly applicable to $Ca + H^+$ collisions.

If the Hamiltonian diabatic matrix is known in the JJ representation, one can calculate the adiabatic potentials with account for the fine structure. Figure 1 shows an example of the adiabatic potentials with and without accounting for the fine structure for molecular states asymptotically correlating with the $Ca^+(4f\,^2F^\circ) + H$ and $Ca^+(6s\,^2S) + H$ scattering channels. One can see that in the LS representation two potentials (dotted lines) create one avoided-crossing region due to the ionic-covalent interaction, while in the JJ representation the system has three molecular states (11, 12, and 13, with account for the fine structure) and these three potentials (solid lines) create two avoided-crossing regions. Thus, the nonadiabatic nuclear dynamics in the fine-structure molecular states is more complicated than the dynamics in non-fine-structure molecular states. Ultimately, this results in different values of state-to-state transition probabilities, inelastic cross sections, and inelastic rate coefficients.

It is noteworthy that the asymptotes of some calculated LS potentials [65,66] deviate from the experimental energies [64]. In order to improve the inelastic cross sections and rate coefficients, we adjusted the diabatic potentials obtained from the *ab initio* adiabatic ones according to their experimental asymptotes, for example, for the $Ca^+(5d\,^2D_{3/2,5/2}) + H(1s\,^2S)$ and $Ca^+(6p\,^2P^\circ_{1/2}) + H(1s\,^2S)$ molecular states. These shifts also affect the parameters of nonadiabatic regions.

Known off-diagonal matrix elements of the electronic Hamiltonian matrix in the JJ representation and, finally, fine-structure adiabatic potentials in avoided-crossing regions allow one to calculate the nonadiabatic transition probabilities by means of the Landau-Zener model in each nonadiabatic region. Originally the model was formulated in a diabatic representation, but if the potentials are known in the adiabatic representation, then the adiabatic-potential-based formula [70] allows one to compute the Landau-Zener probabilities from information about adiabatic potentials only. In the present work the Landau-Zener parameters are calculated via the off-diagonal matrix elements, Eq. (3). With the long-range nonadiabatic regions located in a particular order, one can use the multichannel formulas for calculating the state-to-state inelastic transition probabilities $P_{kn}(E, J_t)$ [27–29], E being a collision energy and J_t a total angular momentum quantum number.

The multichannel Landau-Zener is applicable when several nonadiabatic regions are located in a particular order, for example, when both the centers and the average potentials of avoided-crossing nonadiabatic regions are continuously increasing (see [27] for details). If so, incoming and, later, outgoing probability currents traverse such nonadiabatic regions in a well-defined order, and it is possible to derive the analytic formulas for the state-to-state inelastic transition probabilities P_{if} for a given initial i and a given final f channel in the multichannel case [27–29]. Assuming that the nonadiabatic regions are separated from each other, one can express P_{if} analytically via the nonadiabatic transition probabilities p_k in each nonadiabatic region k after a single traverse of this region (see [27–29], and references therein). If the probabilities p_k are evaluated by means of the Landau-Zener model, the approach is called the multichannel Landau-Zener. The multichannel Landau-Zener approach accounting for both tunneling and probability-current oscillations is employed in the present work.

Inelastic cross sections and rate coefficients can then be calculated in the usual way as follows. For exothermic processes $k \to n$ (we consider excitation energies $E_k > E_n$), the cross sections $\sigma_{kn}(E)$ and the rate coefficients $K_{kn}(T)$ are computed by the formulas

$$\sigma_{kn}(E) = \frac{\pi\hbar^2 p_k^{\rm stat}}{2\mu E} \sum_{J_t=0}^{\infty} P_{kn}(E, J_t)\,(2J_t + 1)\,, \tag{6}$$

$$K_{kn}(T) = \sqrt{\frac{8}{\pi\,\mu(k_B T)^3}} \int_0^{\infty} E\,\sigma_{kn}(E)\,\exp\left(-\frac{E}{k_B T}\right) dE\,, \tag{7}$$

where $p_k^{\rm stat}$ is the statistical probability for the population of channel k, μ is the reduced nuclear mass, T is the temperature, and k_B is the Boltzmann constant. For endothermic processes $n \to k$, the cross sections $\sigma_{nk}(E)$ and the rate coefficients $K_{nk}(T)$ can be calculated by the detailed balance expressions

$$\sigma_{nk}(E) = \sigma_{kn}(E - \Delta E_{kn})\,\frac{p_n^{\rm stat}}{p_k^{\rm stat}}\,\frac{E - \Delta E_{kn}}{E}\,, \tag{8}$$

$$K_{nk}(T) = K_{kn}(T)\,\frac{p_n^{\rm stat}}{p_k^{\rm stat}}\,\exp\left(-\frac{\Delta E_{kn}}{k_B T}\right), \tag{9}$$

$\Delta E_{kn} = E_k - E_n$ being an energy defect between channel k and channel n.

III. $Ca^+ + H$ AND $Ca^{2+} + H^-$ COLLISIONS

A. Fine-structure treatment

In the present work, the cross sections and rate coefficients are calculated for the excitation, de-excitation, neutralization, and ion-pair formation processes in $Ca^+ + H$ and $Ca^{2+} + H^-$ collisions taking the fine structure into account for the collision energy range from 10^{-4} to 100 eV and for the temperature range from 1000 to 10 000 K. The calculated rates are available upon request. In addition, Fig. 2 shows a graphical representation of the calculated rates at temperature $T = 6000$ K, and the most valuable rates at the same temperature are listed in Table III (for the channels $k = 6$–18 and 22).

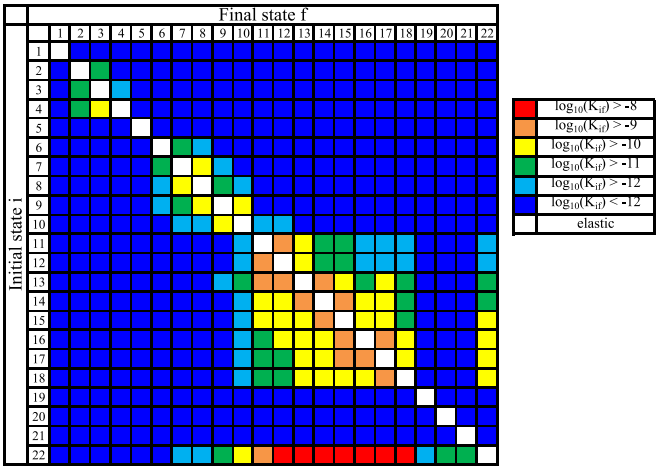

FIG. 2. Graphical representation of the rate coefficients for the partial processes of excitation, de-excitation, neutralization, and ion-pair formation in $Ca^+ + H$ and $Ca^{2+} + H^-$ collisions at temperature $T = 6000$ K. The key labels are presented in Table I.

Similarly to other processes in collisions with hydrogen, the computed rate coefficients can be separated into three groups:

(i) rate coefficients with the highest values (exceeding 10^{-8} cm^3 s^{-1}; red squares in Fig. 2);

(ii) rate coefficients with moderate values (between 10^{-12} and 10^{-8} cm^3 s^{-1}; orange, yellow, green, and light-blue squares in Fig. 2); and

(iii) rate coefficients with low values (less than 10^{-12} cm^{3}s^{-1}; blue squares in Fig. 2).

The first group consists of neutralization processes with the final scattering channels from $Ca^+(4f\,^2F^\circ_{7/2}) + H(1s\,^2S_{1/2})$ to $Ca^+(7s\,^2S_{1/2}) + H(1s\,^2S_{1/2})$ (channels $k = 12$–18 in Table I) with values from 1.11×10^{-8} to 9.21×10^{-8} cm^3 s^{-1} at temperature $T = 6000$ K. The highest rate corresponds to the neutralization in the final channel $Ca^+(6p\,^2P^\circ_{3/2}) + H(1s\,^2S_{1/2})$ ($k = 17$). These neutralization processes are based on the long-range ionic-covalent interaction mechanism with the final-channel binding energies from the optimal reaction window (see [25] and [26] for details).

The second group consists of many processes of excitation, de-excitation, neutralization, and ion-pair formation. At temperature $T = 6000$ K, the highest rate coefficients from this group correspond to the (de-)excitation processes $13 \to 12$, $13 \to 11$, $16 \to 15$, $16 \to 17$, $14 \to 15$, $15 \to 14$, $14 \to 13$, $13 \to 14$, $12 \to 11$, $11 \to 12$, $18 \to 17$, $22 \to 11$, $17 \to 15$, and $17 \to 16$, with the values exceeding 10^{-9} cm^3 s^{-1} (see Table I for the labels and Table III for the rates). The highest (de-)excitation rate, with the value 5.61×10^{-9} cm^3 s^{-1} at $T = 6000$ K, corresponds to the process $Ca^+(6s\,^2S_{1/2}) + H(1s\,^2S_{1/2}) \to Ca^+(4f\,^2F^\circ_{7/2}) + H(1s\,^2S_{1/2})$ ($13 \to 12$). The highest (de-)excitation rate is one order of magnitude lower than the highest neutralization rate. The processes in the second group are also mainly based on the long-range ionic-covalent reaction mechanism, with binding energies for both the initial and the final scattering channels belonging to the optimal window (see Fig. 2 and Table III). The processes in these two groups are the most important for non-LTE applications.

The third group consists of processes involving the ground-state channel, $k = 1$, the low-lying channels 2–5 [except several (de-)excitation processes], the high-excited channels 19–21 (but not the neutralization into these channels), and some others with rates below 10^{-12} cm^3 s^{-1}. It should be noted that the rate coefficients for these processes may show a significant increase (up to several orders of magnitude) due to the loop reaction mechanism if short-range nonadiabatic regions are taken into account, as shown in [31]. High-lying states are more sensitive to these effects, because usually there are many nonadiabatic regions created by high-lying states.

An interesting feature is the dependence of the rate coefficients on the excitation energies of the Ca II ion in the final scattering channels $Ca^+(nl\,^2L_j) + H$. Such a dependence for the neutralization processes, the processes with the highest rate coefficients, with accounting for the fine structure (that is, in the JJ representation) is plotted by open triangles in Fig. 3 for the temperature $T = 6000$ K. It is shown that the rate

TABLE III. Rate coefficients for the inelastic processes in $Ca^+ + H$ and $Ca^{2+} + H^-$ collisions between the scattering channels $k = 6$–18 and $k = 22$ at $T = 6000$ K. The key labels are listed in Table I. Numbers in Square brackets represent the power of 10.

	6	7	8	9	10	11	12	13	14	15	16	17	18	22
6	—	5.14[−11]	6.33[−12]	4.51[−13]	3.62[−14]	1.04[−16]	9.57[−17]	8.91[−17]	3.55[−17]	3.23[−17]	3.95[−18]	7.18[−18]	1.05[−18]	2.01[−17]
7	7.88[−11]	—	2.75[−10]	9.83[−12]	5.48[−13]	1.04[−15]	9.27[−16]	8.25[−16]	3.09[−16]	2.70[−16]	3.35[−17]	6.07[−17]	9.04[−18]	1.29[−16]
8	6.50[−12]	1.85[−10]	—	4.64[−11]	1.84[−12]	2.62[−15]	2.28[−15]	1.98[−15]	7.13[−16]	6.07[−16]	7.59[−17]	1.37[−16]	2.07[−17]	2.56[−16]
9	3.35[−12]	4.77[−11]	3.36[−10]	—	2.31[−10]	1.72[−13]	1.43[−13]	1.16[−13]	3.86[−14]	3.14[−14]	3.94[−15]	7.10[−15]	1.08[−15]	1.02[−14]
10	1.37[−13]	1.35[−12]	6.80[−12]	1.18[−10]	—	1.40[−12]	1.06[−12]	7.72[−13]	2.24[−13]	1.70[−13]	2.13[−14]	3.80[−14]	5.72[−15]	4.02[−14]
11	1.56[−15]	1.02[−14]	3.84[−14]	3.48[−13]	5.56[−12]	—	1.51[−09]	5.00[−10]	7.90[−11]	4.35[−11]	4.84[−12]	8.21[−12]	1.10[−12]	3.59[−12]
12	1.08[−15]	6.83[−15]	2.51[−14]	2.17[−13]	3.17[−12]	1.17[−09]	—	7.18[−10]	9.62[−11]	5.07[−11]	5.53[−12]	9.34[−12]	1.23[−12]	3.88[−12]
13	7.54[−15]	4.56[−14]	1.63[−13]	1.32[−12]	1.73[−11]	2.99[−09]	5.61[−09]	—	1.87[−09]	9.31[−10]	9.53[−11]	1.58[−10]	2.00[−11]	5.76[−11]
14	2.45[−15]	1.40[−14]	4.79[−14]	3.59[−13]	4.09[−12]	3.63[−10]	5.90[−10]	1.63[−09]	—	2.58[−09]	2.04[−10]	3.23[−10]	3.47[−11]	7.41[−11]
15	1.49[−15]	8.13[−15]	2.73[−14]	1.95[−13]	2.07[−12]	1.33[−10]	2.07[−10]	5.09[−10]	1.73[−09]	—	4.14[−10]	6.23[−10]	5.78[−11]	1.05[−10]
16	8.35[−16]	4.62[−15]	1.56[−14]	1.12[−13]	1.19[−12]	6.79[−11]	1.04[−10]	2.39[−10]	6.38[−10]	1.96[−09]	—	5.41[−09]	2.45[−10]	2.06[−10]
17	7.65[−16]	4.22[−15]	1.43[−14]	1.02[−13]	1.07[−12]	5.85[−11]	8.87[−11]	2.02[−10]	5.06[−10]	1.45[−09]	2.73[−09]	—	2.51[−10]	2.17[−10]
18	7.34[−16]	4.16[−15]	1.42[−14]	1.02[−13]	1.06[−12]	5.11[−11]	7.63[−11]	1.65[−10]	3.51[−10]	8.74[−10]	8.09[−10]	1.64[−09]	—	8.15[−10]
22	6.47[−13]	2.72[−12]	8.01[−12]	4.42[−11]	3.42[−10]	7.67[−09]	1.11[−08]	2.19[−08]	3.45[−08]	7.30[−08]	4.62[−08]	9.21[−08]	3.90[−08]	—

coefficient dependence has a maximum for the $Ca^+(6p\,^2P^\circ_{3/2})$ state and decreases in both directions. This is a general form for such dependences [25,26]. The maximum for this particular final channel is the result of the fact that the binding energy of Ca II in this channel is located in the most optimal window. This fact confirms that the reaction mechanism of the neutralization processes with large-valued rates corresponds to the long-range ionic-covalent interaction. Accounting for the fine structure yields a scatter of the rates, since the rates of the Ca II fine-structure levels have different values. The ratios between the rates of the fine-structure levels are also different for different Ca II states (see Fig. 3). This is the result of relation (3), which determines the Landau-Zener parameters and the CaH^+ electronic structure in the JJ representation.

The similar dependence of the rate coefficients on the excitation energies of the Ca II states in the final scattering channels for the (de-)excitation processes is shown in Fig. 4; the initial scattering channel is $Ca^+(6p\,^2P^\circ_{1/2}) + H$. This dependence is in agreement with the general dependence predicted by the simplified model [25,26]. The maximal values for the (de-)excitation processes from this initial channel correspond to the final channels $Ca^+(6p\,^2P_{3/2}) + H$ (the transition between the fine-structure levels) and $Ca^+(5d\,^2D_{5/2}) + H$, and this is the result of the fact that the excitation energies of the $Ca^+(6p\,^2P_{3/2})$ and $Ca^+(5d\,^2D_{5/2})$ states belong to the most optimal window as well, and hence, the reaction mechanism also corresponds to the long-range ionic-covalent interaction.

As mentioned in Sec. I, the Ca II infrared triplet 849.8/854.2/866.2 nm is of particular interest. It corresponds to the transitions between the fine-structure

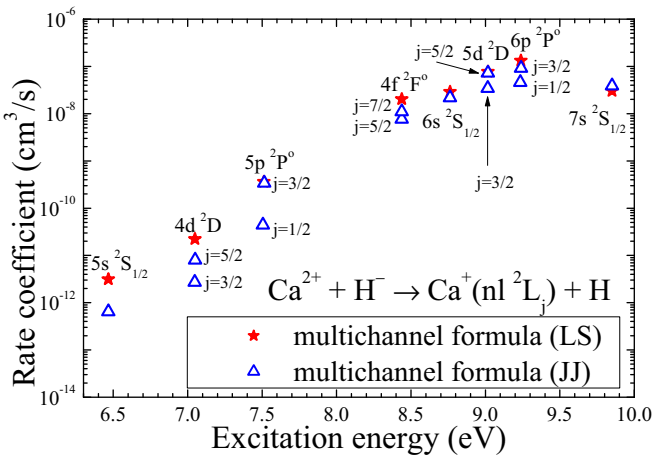

FIG. 3. Rate coefficients for the neutralization processes at $T = 6000$ K as a function of the excitation energy of the Ca^+ ion (measured from the ground-state level) in the final channels. The rates are computed in the JJ (open blue triangles) and in the LS (red stars) representations, that is, with and without accounting for the fine structure. The calculations are performed by the multichannel Landau-Zener approach.

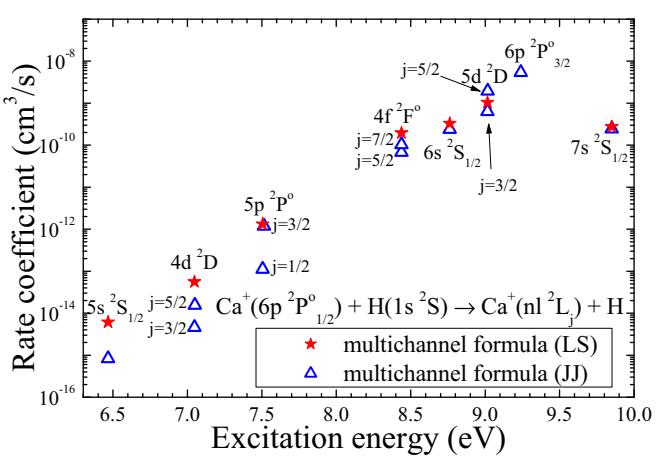

FIG. 4. Rate coefficients for the de-excitation and excitation processes as a function of the excitation energy of the Ca^+ ion in the final channels at $T = 6000$ K. The rates are calculated in the JJ (open blue triangles) and in the LS (red stars) representations, that is, with and without account for the fine structure. The initial channel is $Ca^+(6p\,^2P^\circ_{1/2}) + H$. The calculations are performed by the multichannel Landau-Zener approach.

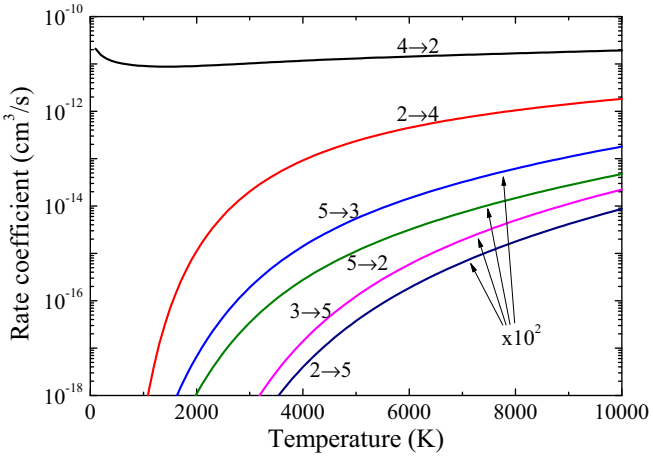

FIG. 5. Temperature dependence for the processes $Ca^+(4p\,^2P^\circ_{3/2}) + H \to Ca^+(3d\,^2D_{3/2}) + H$ (transition $5 \to 2$), $Ca^+(4p\,^2P^\circ_{3/2}) + H \to Ca^+(3d\,^2D_{5/2}) + H$ (transition $5 \to 3$), and $Ca^+(4p\,^2P^\circ_{1/2}) + H \to Ca^+(3d\,^2D_{3/2}) + H$ (transition $4 \to 2$) and their inverses.

states: $Ca^+(4p\,^2P^\circ_{3/2}) \to Ca^+(3d\,^2D_{3/2})$ (the transition $5 \to 2$), $Ca^+(4p\ ^2P^\circ_{3/2}) \to Ca^+(3d\,^2D_{5/2})$ ($5 \to 3$), and $Ca^+(4p\,^2P^\circ_{1/2}) \to Ca^+(3d\,^2D_{3/2})$ ($4 \to 2$). For this reason, the inelastic processes in collisions of calcium ions with hydrogen atoms leading to transitions between these fine-structure states are of importance. Figure 5 presents the temperature dependence of the rate coefficients of the processes for the Ca II triplet transitions in collisions with H and their inverses. One can see that the rate for the $4 \to 2$ de-excitation process weakly depends on the temperature, while the others depend strongly on it. It is shown that the rate coefficients for these processes are mainly low, although one process has a moderate rate, namely, the de-excitation process $4 \to 2$, with the maximum slightly exceeding the value of 1.4×10^{-11} cm^3 s^{-1} at $T = 6000$ K.

The calculated rate coefficients at $T = 6000$ K for the excitation and de-excitation processes with transitions between the low-lying fine-structure channels 2–5 are listed in Table IV, including the Ca II infrared triplet transitions. One can see that the rate coefficients of these processes are low as well; only one of them has the moderate value of 1.62×10^{-10} cm^3 s^{-1} (the $4 \to 3$ transition), several processes have rates exceeding the value of 10^{-11} cm^3 s^{-1} ($2 \to 3$, $3 \to 2$, and $4 \to 2$), and the others are much lower. The low values of the rate coefficients for the processes with transitions between the low-lying

TABLE IV. Rate coefficients for (de-)excitation processes involving scattering channels 2–5 at $T = 6000$ K. The key labels are listed in Table I. Numbers in Square brackets represent the power of 10.

	2	3	4	5
2	—	3.58[−11]	4.49[−13]	1.87[−18]
3	2.42[−11]	—	3.45[−12]	5.84[−18]
4	1.43[−11]	1.62[−10]	—	3.96[−15]
5	3.15[−17]	1.46[−16]	2.10[−15]	—

states are the results of large splittings between the *LS* adiabatic potentials. In particular, the adiabatic-potential splitting in the center of a nonadiabatic region between the *LS* states $Ca^+(4p\,^2P^\circ) + H$ and $Ca^+(5s\,^2S) + H$ is ≈ 2.245 eV. This large energy gap cuts off the lowest-lying states ($k \leqslant 5$) from other states, which are above the $Ca^+(5s\,^2S) + H$ state ($k = 6$) in the *LS* representation. The minimal energy splitting between the ground-state potential ($k = 1$) and the first-excited-state potential ($k = 2$) is ≈ 1.55 eV, and this gap separates the ground state from other states. In the *JJ* representation, the fine-structure levels split and the adiabatic-potential splitting in the center of the nonadiabatic region between the fine-structure states $Ca^+(4p\,^2P^\circ_{1/2}) + H$ and $Ca^+(4p\,^2P^\circ_{3/2}) + H$ is ≈ 1.587 eV. This leads to large values for the off-diagonal matrix elements [see Eq. (3)] and, finally, to low transition probabilities, low inelastic cross sections, and low rate coefficients for the processes $Ca^+(4p\,^2P^\circ_{3/2}) + H \to Ca^+(3d\,^2D_{3/2,5/2}) + H$, the processes corresponding to the Ca II infrared triplet transitions (see Fig. 5 and Table IV).

B. Comparison of rate coefficients with and without account for the fine structure

The rate coefficients for the inelastic processes in $Ca^+ + H$ and $Ca^{2+} + H^-$ collisions calculated in the present work accounting for the fine structure should be compared with the rates computed without accounting for the fine structure. The latter are calculated in [31] in the *LS* representation by means of both the multichannel Landau-Zener approach and the probability current method. The results for the neutralization processes are presented in Figs. 3 and 6. Figures 4 and 7 show a similar comparison for the (de-)excitation rate coefficients calculated with and without accounting for the fine structure. First, one can see in Figs. 6 and 7 that the large-valued rate coefficients [for processes with the final channels higher than the channel $Ca^+(5p\,^2P) + H$] calculated by the multichannel

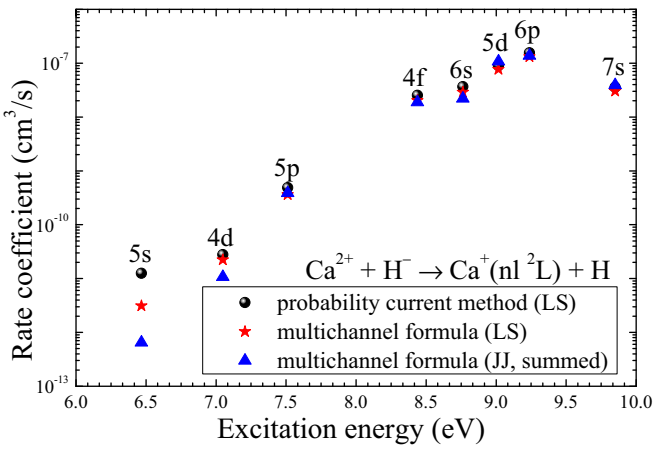

FIG. 6. Comparison of the rate coefficients for neutralization processes at $T = 6'00$ K as a function of the excitation energy of the Ca^+ ion in the final channels for the three data sets: (i) rates obtained by the probability current method in the *LS* representation (black circles); (ii) rates computed by the multichannel approach in the *LS* representation (red stars); and (iii) rates calculated by the multichannel approach in the *JJ* representation and summed over fine-structure states (blue triangles).

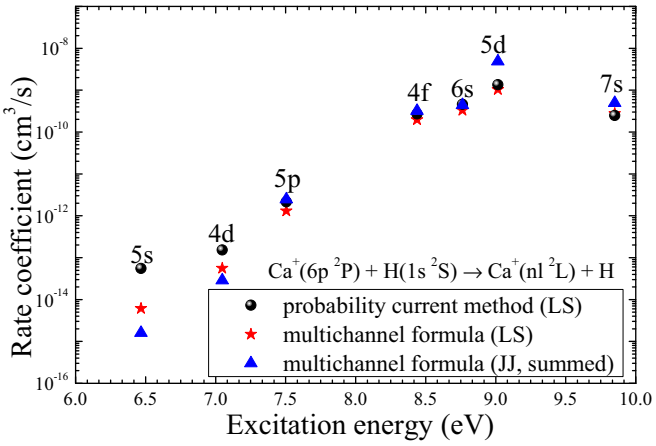

FIG. 7. Comparison of the rate coefficients for the de-excitation and excitation processes at $T = 6000$ K as a function of the excitation energy of the Ca^+ ion in the final channels for the results obtained by (i) the probability current method in the *LS* representation (black circles), (ii) the multichannel Landau-Zener approach in the *LS* representation (red stars), and (iii) the multichannel Landau-Zener approach in the *JJ* representation and summed over fine-structure states (blue triangles), that is, with and without accounting for the fine structure. The initial channels are $Ca^+(6p\,^2P^\circ_{1/2,3/2}) + H$, and the fine-structure results are summed over the fine-structure levels of the initial and the final channels.

approach agree well with the rates calculated by the probability current method. This means that the dominant mechanism for the processes with large-valued rates is the long-range ionic-covalent interaction. The processes with lower-lying final channels, below the channel $Ca^+(5p\,^2P) + H$, have rates calculated by the probability current method larger than those calculated by the multichannel approach. The point is that the multichannel approach takes into account only long-range nonadiabatic regions, while the probability current method accounts for both short- and long-range nonadiabatic regions, and this affects the rates for transitions between low-lying states, especially rates with low values. Nevertheless, the multichannel approach yields reasonable rate coefficients for important processes.

Second, it is shown in Figs. 6 and 7 that there are different cases in comparison of the rates obtained by the multichannel approach with and without accounting for the fine structure: for some processes the rates obtained with and without accounting for fine structure are approximately equal [e.g., for the $5p$ (neutralization), $4f$, and $6p$ states], for some processes the rates with fine structure are lower than those without fine structure (e.g., for $5s$, $4d$, and $6s$), and for some others the rates with fine structure are higher than the rates without fine structure [e.g., for $5p$ (de-excitation), $5d$, and $7s$]. Sometimes the rate coefficient for one of two fine-structure processes is higher than the rate for the corresponding *LS* state (see Figs. 3 and 4, e.g., for the $5d$ state).

As mentioned in Sec. I, the common way to take the fine structure into account in collisions with hydrogen consists in redistributing the collisional rate between fine-structure levels. The present calculations and analysis show that such a redistribution could be fulfilled accidentally, but this is not a general rule. The correct way to take the fine structure into account consists in performing a dynamical calculation based on an electronic structure constructed in the *JJ* representation. One should also note the different statistical probabilities $p_k^{\rm stat}$ for populations of molecular states of the 0^+ and of the $^1\Sigma^+$ symmetries, that is, in the *JJ* and in the *LS* representations.

IV. CONCLUSIONS

The present paper reports the developed method for taking the fine structure into account in collisions of alkaline atoms and alkaline-like ions with hydrogen, as well as the application of the method to the processes in $Ca^+ + H$ and $Ca^{2+} + H^-$ collisions. The method is based on the modification of the adiabatic potentials by switching the representation from the *LS* to the *JJ* coupling scheme. The key point of this transformation is the determination of the off-diagonal matrix elements of the ionic-covalent interaction in the *JJ* representation via similar elements in the *LS* representation. It turns out that these matrix elements are proportional to each other [69] [see Eq. (3)].

The *ab initio* potentials for the 13 covalent $Ca^+ + H$ states of $^1\Sigma^+$ molecular symmetry and the one ionic $Ca^{2+} + H^-$ state of the same symmetry calculated in the *LS* representation are taken from [65] and [66]. These potentials are used for construction of the adiabatic potentials for the 22 molecular states of 0^+ symmetry in the *JJ* representation taking the fine structure of Ca^+ and $H(2p)$ into account. Then the nonadiabatic nuclear dynamics is studied on the constructed 0^+ potentials by means of the multichannel Landau-Zener approach for the collisional energy range 10^{-4} to 100 eV. Finally, the rate coefficients are calculated for the temperature range 1000 to 10 000 K.

The treated processes in $Ca^+ + H$ and $Ca^{2+} + H^-$ collisions can be separated into three groups: (i) processes with the largest rate coefficients, typically exceeding the value of 10^{-8} cm^3 s^{-1}; (ii) processes with moderate rates, between 10^{-12} and 10^{-8} cm^3 s^{-1}; and (iii) processes with low rates, below 10^{-12} cm^3 s^{-1}.

It is found that the largest rate coefficients correspond to the neutralization processes in the final channels $Ca^+(4f\,^2F^\circ_{7/2})$, $Ca^+(6s\,^2S_{1/2})$, $Ca^+(5d\,^2D_{3/2,5/2})$, $Ca^+(6p\,^2P^\circ_{1/2,3/2})$, and $Ca^+(7s\,^2S_{1/2}) + H(1s\,^2S_{1/2})$ and have values in the range $(1.11\text{–}9.21) \times 10^{-8}$ cm^3 s^{-1} at temperature 6000 K. It is shown that the reaction mechanism for these processes corresponds to the long-range ionic-covalent interaction. It is also shown that accounting for the fine structure does not lead to a simple redistribution of rate coefficients obtained within the *LS* coupling scheme between the fine-structure levels.

The rate coefficients for the Ca II infrared triplet 849.8/854.2/866.2-nm transitions in collisions with H are found to be small. The only moderate rate coefficient is found in the range 9.06×10^{-12} to 1.93×10^{-11} cm^3 s^{-1} for temperatures between 1000 and 10 000 K and corresponds to the transition $Ca^+(4p\,^2P^\circ_{1/2}) \rightarrow Ca^+(3d\,^2D_{3/2})$ in H collisions.

The rate coefficients for the transitions $Ca^+(4p\,^2P^\circ_{3/2}) \leftrightarrow Ca^+(3d\,^2D_{3/2,5/2})$ are found to have values below 1.8×10^{-15} cm^3 s^{-1} for the treated temperature range.

Processes with large and moderate values of the rate coefficients are likely to be important in non-LTE modeling of stellar atmospheres.

Supplemental Material present the calculated rate coefficients (in units of cm^3 s^{-1}) for the inelastic processes in $Ca^+ + H$ and $Ca^{2+} + H^-$ collisions for temperatures from $T = 1000$ K to $T = 10\,000$ K [71].

ACKNOWLEDGMENTS

The authors gratefully acknowledge support from the Russian Science Foundation (Russian Federation) (Grant No. 17-13-01144).

[1] M. Asplund, Annu. Rev. Astron. Astrophys. **43**, 481 (2005).
[2] L. Mashonkina, Phys. Scripta **134**, 014004 (2009).
[3] L. Mashonkina, in *Setting the scene for Gaia and LAMOST*, *IAU Symposium*, Vol. 298, edited by S. Feltzing, G. Zhao, N. A. Walton, and P. Whitelock (International Astronomical Union, Paris, 2014), pp. 355–365.
[4] P. S. Barklem, Astron. Astrophys. Rev. **24**, 9 (2016).
[5] H.-W. Drawin, Z. Phys. **211**, 404 (1968).
[6] H.-W. Drawin, Z. Phys. **225**, 483 (1969).
[7] W. Steenbock and H. Holweger, A&A **130**, 319 (1984).
[8] P. S. Barklem, A. K. Belyaev, M. Guitou, N. Feautrier, F. X. Gadéa, and A. Spielfiedel, A&A **530**, A94 (2011).
[9] A. K. Belyaev, J. Grosser, J. Hahne, and T. Menzel, Phys. Rev. A **60**, 2151 (1999).
[10] H. Croft, A. S. Dickinson, and F. X. Gadéa, J. Phys. B: At. Mol. Opt. Phys. **32**, 81 (1999).
[11] H. Croft, A. S. Dickinson, and F. X. Gadéa, Mon. Not. R. Astron. Soc. **304**, 327 (1999).
[12] A. K. Belyaev and P. S. Barklem, Phys. Rev. A **68**, 062703 (2003).
[13] M. Stenrup, A. Larson, and N. Elander, Phys. Rev. A **79**, 012713 (2009).
[14] A. K. Belyaev, P. S. Barklem, A. S. Dickinson, and F. X. Gadéa, Phys. Rev. A **81**, 032706 (2010).
[15] A. K. Belyaev, P. S. Barklem, A. Spielfiedel, M. Guitou, N. Feautrier, D. S. Rodionov, and D. V. Vlasov, Phys. Rev. A **85**, 032704 (2012).
[16] A. K. Belyaev, D. V. Vlasov, A. Mitrushchenkov, and N. Feautrier, Mon. Not. R. Astron. Soc. **490**, 3384 (2019).
[17] M. Guitou, A. K. Belyaev, P. S. Barklem, A. Spielfiedel, and N. Feautrier, J. Phys. B **44**, 035202 (2011).
[18] M. Guitou, A. Spielfiedel, D. S. Rodionov, S. A. Yakovleva, A. K. Belyaev, T. Merle, F. Thevenin, and N. Feautrier, Chem. Phys. **462**, 94 (2015).
[19] A. K. Belyaev, Phys. Rev. A **91**, 062709 (2015).
[20] S. M. Nkambule, N. Elander, A. Larson, J. Lecointre, and X. Urbain, Phys. Rev. A **93**, 032701 (2016).
[21] A. Mitrushchenkov, M. Guitou, A. K. Belyaev, S. A. Yakovleva, A. Spielfiedel, and N. Feautrier, J. Chem. Phys. **146**, 014304 (2017).
[22] A. K. Belyaev, Phys. Rev. A **88**, 052704 (2013).
[23] P. S. Barklem, Phys. Rev. A **93**, 042705 (2016).
[24] P. S. Barklem, Phys. Rev. A **95**, 069906(E) (2017).
[25] A. K. Belyaev and S. A. Yakovleva, A&A **606**, A147 (2017).
[26] A. K. Belyaev and S. A. Yakovleva, A&A **608**, A33 (2017).
[27] A. K. Belyaev, Phys. Rev. A **48**, 4299 (1993).
[28] A. K. Belyaev, S. A. Yakovleva, and P. S. Barklem, A&A **572**, A103 (2014).
[29] S. A. Yakovleva, Y. V. Voronov, and A. K. Belyaev, A&A **593**, A27 (2016).
[30] A. K. Belyaev, Y. V. Voronov, S. A. Yakovleva, A. Mitrushchenkov, M. Guitou, and N. Feautrier, Astrophys. J. **851**, 59 (2017).
[31] A. K. Belyaev, Y. V. Voronov, and F. X. Gadéa, Astrophys. J. **867**, 87 (2018).
[32] S. A. Yakovleva, A. K. Belyaev, and W. P. Kraemer, Chem. Phys. **515**, 369 (2018).
[33] P. S. Barklem, A&A **610**, A57 (2018).
[34] A. Mitrushchenkov, M. Guitou, A. K. Belyaev, Y. V. Voronov, and N. Feautrier, J. Chem. Phys. **150**, 064312 (2019).
[35] A. K. Belyaev, Y. V. Voronov, A. Mitrushchenkov, M. Guitou, and N. Feautrier, Mon. Not. R. Astron. Soc. **487**, 5097 (2019).
[36] A. M. Amarsi and P. S. Barklem, A&A **625**, A78 (2019).
[37] Y. Osorio, K. Lind, P. S. Barklem, C. Allende Prieto, and O. Zatsarinny, A&A **623**, A103 (2019).
[38] E. Terlevich, A. I. Diaz, and R. Terlevich, Astrophys. Space. Sci. **157**, 15 (1989).
[39] G. Kordopatis, A. Recio-Blanco, P. de Laverny, A. Bijaoui, V. Hill, G. Gilmore, R. F. G. Wyse, and C. Ordenovic, A&A **535**, A106 (2011).
[40] E. Starkenburg, V. Hill, E. Tolstoy, J. I. González Hernández, M. Irwin, A. Helmi, G. Battaglia, P. Jablonka, M. Tafelmeyer, M. Shetrone, K. Venn, and T. de Boer, A&A **513**, A34 (2010).
[41] G. S. Da Costa, Mon. Not. R. Astron. Soc. **455**, 199 (2016).
[42] L. Mashonkina, A. J. Korn, and N. Przybilla, A&A **461**, 261 (2007).
[43] L. Mashonkina, T. Sitnova, and A. K. Belyaev, A&A **605**, A53 (2017).
[44] T. M. Sitnova, L. I. Mashonkina, and T. A. Ryabchikova, Mon. Not. R. Astron. Soc. **477**, 3343 (2018).
[45] P. E. Nissen and W. J. Schuster, A&A **511**, L10 (2010).
[46] T. Bensby, J. C. Yee, S. Feltzing, J. A. Johnson, A. Gould, J. G. Cohen, M. Asplund, J. Meléndez, S. Lucatello, C. Han, I. Thompson, A. Gal-Yam, A. Udalski, D. P. Bennett, I. A. Bond, W. Kohei, T. Sumi, D. Suzuki, K. Suzuki, S. Takino, P. Tristram, N. Yamai, and A. Yonehara, A&A **549**, A147 (2013).
[47] J. J. Drake, Mon. Not. R. Astron. Soc. **251**, 369 (1991).
[48] T. Idiart and F. Thévenin, Astrophys. J. **541**, 207 (2000).
[49] N. Christlieb, M. S. Bessell, T. C. Beers, B. Gustafsson, A. Korn, P. S. Barklem, T. Karlsson, M. Mizuno-Wiedner, and S. Rossi, Nature **419**, 904 (2002).
[50] A. Frebel, W. Aoki, N. Christlieb, H. Ando, M. Asplund, P. S. Barklem, T. C. Beers, K. Eriksson, C. Fechner, M. Y. Fujimoto, S. Honda, T. Kajino, T. Minezaki, K. Nomoto, J. E. Norris, S. G. Ryan, M. Takada-Hidai, S. Tsangarides, and Y. Yoshii, Nature **434**, 871 (2005).

[51] J. Norris, N. Christlieb, A. Korn, K. Eriksson, M. S. Bessell, T. C. Beers, L. Wisotzki, and D. Reimers, Astrophys. J. **670**, 774 (2007).

[52] A. J. Korn, O. Richard, L. Mashonkina, M. S. Bessell, A. Frebel, and W. Aoki, Astrophys. J. **698**, 410 (2009).

[53] E. Caffau, P. Bonifacio, P. Francois, L. Sbordone, L. Monaco, M. Spite, F. Spite, H.-G. Ludwig, R. Cayrel, S. Zaggia, F. Hammer, S. Randich, P. Molaro, and V. Hill, Nature **477**, 67 (2011).

[54] J. G. Cohen, N. Christlieb, I. Thompson, A. McWilliam, S. Shectman, D. Reimers, L. Wisotzki, and E. Kirby, Astrophys. J. **778**, 56 (2013).

[55] A. Frebel, A. Chiti, A. P. Ji, H. R. Jacobson, and V. M. Placco, Astrophys. J. **810**, L27 (2015).

[56] T. Nordlander, A. M. Amarsi, K. Lind, M. Asplund, P. S. Barklem, A. R. Casey, R. Collet, and J. Leenaarts, A&A **597**, A6 (2017).

[57] T. Merle, F. Thévenin, B. Pichon, and L. Bigot, Mon. Not. R. Astron. Soc. **418**, 863 (2011).

[58] T. Merle, F. Thévenin, B. Pichon, and L. Bigot, in *SF2A-2012: Proceedings of the Annual Meeting of the French Society of Astronomy and Astrophysics*, edited by S. Boissier, P. de Laverny, N. Nardetto, R. Samadi, D. Valls-Gabaud, and H. Wozniak (FSAA, Hyderabad, India, 2012) pp. 369–373.

[59] M. Spite, S. M. Andrievsky, F. Spite, E. Caffau, S. A. Korotin, P. Bonifacio, H.-G. Ludwig, P. François, and R. Cayrel, A&A **541**, A143 (2012).

[60] K. Lind, J. Melendez, M. Asplund, R. Collet, and Z. Magic, A&A **554**, A96 (2013).

[61] C. Siqueira-Mello, S. M. Andrievsky, B. Barbuy, M. Spite, F. Spite, and S. A. Korotin, A&A **584**, A86 (2015).

[62] A. K. Belyaev, S. A. Yakovleva, M. Guitou, A. O. Mitrushchenkov, A. Spielfiedel, and N. Feautrier, A&A **587**, A114 (2016).

[63] P. S. Barklem, A&A **462**, 781 (2007).

[64] A. Kramida, Y. Ralchenko, J. Reader, and NIST ASD Team, *NIST Atomic Spectra Database (Version 5.6)* (National Institute of Standards and Technology, Gaithersburg, MF, 2018); http://physics.nist.gov/asd.

[65] H. Habli, H. Ghalla, B. Oujia, and F. X. Gadéa, Eur. Phys. J. D **64**, 5 (2011).

[66] H. Habli, R. Dardouri, B. Oujia, and F. X. Gadéa, J. Phys. Chem. A **115**, 14045 (2011).

[67] E. E. Nikitin and S. Y. Umanskii, *Theory of Slow Atomic Collisions* (Springer-Verlag, Berlin, 1984) p. 432.

[68] R. E. Olson, F. T. Smith, and E. Bauer, Appl. Opt. **10**, 1848 (1971).

[69] S. A. Yakovleva, Y. V. Voronov, and A. K. Belyaev, Opt. Spectrosc. **127**, 207 (2019).

[70] A. K. Belyaev and O. V. Lebedev, Phys. Rev. A **84**, 014701 (2011).

[71] See Supplemental Material at http://link.aps.org/supplemental/10.1103/PhysRevA.100.062710 for the calculated rate coefficients (in units of $cm^3\,s^{-1}$) for the inelastic processes in $Ca^+ + H$ and $Ca^{2+} + H^-$ collisions for temperatures 1000 to 10 000 K. The JJ*.dat files contain the rates taking the fine structure into account, while the LS*.dat files contain rates that do not consider the fine structure.